単一縞情報を用いた3次元計測のための ブランチカット型符号推定法

○北原 大地　山田 功 （東京工業大学）

A Branch Cut Type Sign Estimator for 3D Measurement from A Single Fringe Pattern

∗D. Kitahara and I. Yamada (Tokyo Institute of Technology)

Abstract– Fringe projection is a technique to measure three-dimensional (3D) shapes of objects by projecting structured light patterns onto the objects. Many fringe projection techniques first compute, by using at least three fringe patterns, the cosine and the sin of the continuous phase distribution which corresponds to the 3D shape of the object, and then estimate the continuous phase by some phase unwrapping algorithm. In the last two decades, for 3D measurement of transient phenomena, reconstruction of the continuous phase from a single fringe pattern has been challenged. In this case, since we can use only the cosine of the continuous phase, we have to estimate sign function of the sine of the continuous phase. In this report, inspired by Goldstein's branch cut phase unwrapping algorithm, we formulate this sign estimation problem as a binary optimization problem, and propose a branch cut type algorithm for solving the optimization problem. Numerical experiments show the effectiveness of the proposed sign estimator compared with a state-of-the-art estimator.

Key Words: Fringe projection, 3D measurement, Fringe analysis, Sign ambiguity resolution, Branch cut type algorithm.

1 Introduction

Fringe projection is a major technique to obtain three-dimensional (3D) surface information of objects in a non-contact manner[1)–3)], and widely used in biomedical[4)–6)], industrial[7)–9)], kinematics[10), 11)], and biometric[12), 13)] applications. A typical fringe projection profilometry system is illustrated in Fig. 1. It consists of a projector, a camera and a digital computer. First, the projector projects sinusoidal fringe patterns onto an object. Second, the camera records images of the fringe patterns which are distorted due to the surface profile of the object. Third, from the recorded images, the digital computer estimates the continuous phase distribution which corresponds to the horizontal projector pixels by using some fringe analysis composed of *wrapped phase detection* and *phase unwrapping* steps. Finally, a 3D surface is computed from the camera pixels and the projector pixels on the basis of triangulation.

A most popular fringe projection technique is the following *three-step phase-shifting method*[14)] because it can obtain 3D information stably from only three simple fringe patterns. Three different fringe images I_k $(k = 1, 2, 3)$, whose phases are shifted by $2\pi/3$ from each other, are recorded on two-dimensional lattice points $(x, y) \in \mathcal{L}$ as

$$\left.\begin{aligned} I_1(x,y) &= a(x,y) + b(x,y)\cos(\phi(x,y)) + n_1(x,y) \\ I_2(x,y) &= a(x,y) + b(x,y)\cos(\phi(x,y) - \tfrac{2\pi}{3}) + n_2(x,y) \\ I_3(x,y) &= a(x,y) + b(x,y)\cos(\phi(x,y) + \tfrac{2\pi}{3}) + n_3(x,y) \end{aligned}\right\}, \tag{1}$$

where $\mathcal{L}$ is the set of all lattice points captured by the camera, a is a slowly varying background illumination, b is the fringe amplitude that is also a low-frequency signal, ϕ is the continuous phase distribution (the so-called *unwrapped phase*) to be estimated, and n_k $(k = 1, 2, 3)$ are independent additive noises. The noisy *wrapped phase*

$$\phi^W(x,y) := W(\phi(x,y) + \nu(x,y)) \in (-\pi, \pi] \tag{2}$$

is computed from $\cos(\phi^W) = \frac{2I_1 - I_2 - I_3}{\sqrt{(2I_1 - I_2 - I_3)^2 + 3(I_2 - I_3)^2}}$ and $\sin(\phi^W) = \frac{\sqrt{3}(I_2 - I_3)}{\sqrt{(2I_1 - I_2 - I_3)^2 + 3(I_2 - I_3)^2}}$, where $\nu \in (-\pi, \pi]$ is phase noise and $W : \mathbb{R} \to (-\pi, \pi]$ is defined by $\forall \varphi \in \mathbb{R}\ \exists \eta \in \mathbb{Z} \quad \varphi = W(\varphi) + 2\pi\eta$ and $W(\varphi) \in (-\pi, \pi]$. ϕ is estimated from ϕ^W by using some two-dimensional phase unwrapping algorithm[15)–18)], and 3D information is obtained from the camera pixel $(x, y) \in \mathcal{L}$ and the horizontal projector pixel $\theta = \phi(x, y)$ by using triangulation.

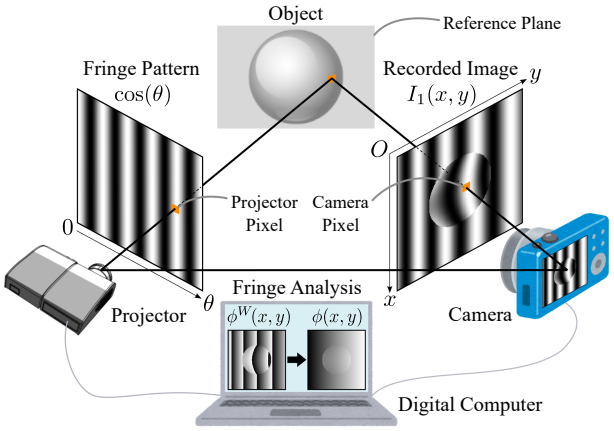

Fig. 1: Typical fringe projection profilometry system

However, the phase-shifting method requires that the physical quantities a, b and ϕ remain constant during the time needed to record the images I_k $(k = 1, 2, 3)$, i.e., a, b and ϕ must be common for all indices $k = 1, 2, 3$ in (1). This condition is not satisfied when transient phenomena are measured[19)] or the environment is hostile. To deal with such situations, reconstruction of ϕ from a single fringe image I_1 in (1) is studied, and several phase recovery algorithms have been proposed[19)–25)]. These algorithms usually use a high pass filter[20)] to remove the background illumination a, and then use Hilbert transform[26)] to normalize the fringe amplitude b. As a result, from I_1 in (1), we can obtain the normalized fringe image

$$I(x,y) = \cos(\phi(x,y) + \nu(x,y)) \in [-1, 1]. \tag{3}$$

From (2) and (3), the absolute value of the wrapped phase is computed as

$$|\phi^W(x,y)| = \arccos(I(x,y)) \in [0,\pi].$$

From $\phi^W(x,y) \in (\pi,\pi]$, we have $\phi^W(x,y) = |\phi^W(x,y)|$ if $|\phi^W(x,y)| = 0$ or $|\phi^W(x,y)| = \pi$, and

$$\phi^W(x,y) = \mathrm{sgn}(\phi^W(x,y))|\phi^W(x,y)| \tag{4}$$

otherwise, where $\mathrm{sgn}(x) := +1$ for $x \geq 0$ and $\mathrm{sgn}(x) := -1$ for $x < 0$. Therefore, in order to compute $\phi^W(x,y)$ for all $(x,y) \in \mathcal{L}$, we have to resolve sign ambiguity in (4).

In this report, on the basis of the discussions in [18], we introduce a minimization problem for the approximated energy of local change of ϕ so that we use a minimizer of the cost function for determination of $\mathrm{sgn}(\phi^W(x,y))$ (see Section 2). For solving this minimization problem, we propose a branch cut type algorithm in Section 3. The word *"branch cut type"* means that the proposed method consists of steps similar to the steps used in Goldstein's branch cut[17], which is a famous two-dimensional phase unwrapping algorithm. Finally, numerical experiments in Section 4 demonstrate the effectiveness of the proposed method compared with the existing method in [23].

2 Minimization of Energy of Local Change for Sign Ambiguity Resolution

Let $\mathcal{L} := \{(x_i,y_j)\}_{j=1,2,\ldots,n}^{i=1,2,\ldots,m}$ s.t. $x_1 < x_2 < \cdots < x_m$ and $y_1 < y_2 < \cdots < y_n$, and let $\Omega := [x_1,x_m] \times [y_1,y_n]$.

By assuming that the normalized image I is noise-free, i.e., $\nu(x,y) = 0$ in (3), the relation between the image gradient $\nabla I(x,y) := (\frac{\partial I}{\partial x}(x,y), \frac{\partial I}{\partial y}(x,y))^T$ and the phase gradient $\nabla\phi(x,y) := (\frac{\partial \phi}{\partial x}(x,y), \frac{\partial \phi}{\partial y}(x,y))^T$ is deduced as

$$\nabla I(x,y) = -\sin(\phi(x,y))\nabla\phi(x,y).$$

As shown above, the orientation of $\nabla\phi(x,y)$ is the same as or opposite to that of $\nabla I(x,y)$ depending on $s(x,y) := \mathrm{sgn}(W(\phi(x,y))) = \mathrm{sgn}(\sin(\phi(x,y)))$. Moreover, on the basis of the idea of *functional data analysis*[18),27)], by trying to minimize the energy of local change of ϕ (defined as the L_2 norm of the second order partial derivative of ϕ):

$$\begin{aligned}
&\iint_\Omega \left[\left| \frac{\partial^2\phi}{\partial x^2} \right|^2 + 2\left| \frac{\partial^2\phi}{\partial x \partial y} \right|^2 + \left| \frac{\partial^2\phi}{\partial y^2} \right|^2 \right] \mathrm{d}x\mathrm{d}y \\
&\approx \sum_{i=1}^{m}\sum_{j=1}^{n-1} \|\nabla\phi(x_i,y_{j+1}) - \nabla\phi(x_i,y_j)\|^2 \\
&\quad + \sum_{i=1}^{m-1}\sum_{j=1}^{n} \|\nabla\phi(x_{i+1},y_j) - \nabla\phi(x_i,y_j)\|^2,
\end{aligned}$$

we introduce the following optimization problem, which is similar to that proposed in [19] for estimation of $s(x_i,y_j)$.

Problem 1 (Approximated energy minimization problem) *Find* $\boldsymbol{S}^* := (s^*_{i,j}) \in \{-1,+1\}^{m\times n}$ *minimizing*

$$\begin{aligned}
J(\boldsymbol{S}) := &\sum_{i=1}^{m}\sum_{j=1}^{n-1} \|s_{i,j+1}\boldsymbol{v}_{i,j+1} - s_{i,j}\boldsymbol{v}_{i,j}\|^2 \\
&+ \sum_{i=1}^{m-1}\sum_{j=1}^{n} \|s_{i+1,j}\boldsymbol{v}_{i+1,j} - s_{i,j}\boldsymbol{v}_{i,j}\|^2,
\end{aligned} \tag{5}$$

where $\boldsymbol{v}_{i,j} := \frac{\nabla I(x_i,y_j)}{\|\nabla I(x_i,y_j)\|}$ *($i = 1,2,\ldots,m$ and $j = 1,2,\ldots,n$) are the normalized image gradient vectors at (x_i,y_j), and $\nabla I(x_i,y_j)$ are approximately computed by applying, e.g., the Prewitt or the Sobel operator, to I in (3).*

After finding a minimizer $\boldsymbol{S}^* = (s^*_{i,j}) \in \{-1,+1\}^{m\times n}$, the wrapped phase ϕ^W at $(x_i,y_j) \in \mathcal{L}$ is estimated by

$$\phi^W(x_i,y_j) = \begin{cases} 0 & \text{if } |\phi^W(x_i,y_j)| = 0; \\ \pi & \text{if } |\phi^W(x_i,y_j)| = \pi; \\ s^*_{i,j}|\phi^W(x_i,y_j)| & \text{otherwise.} \end{cases}$$

Remark 1 *There are at least two minimizers of (5) because $J(\boldsymbol{S}) = J(-\boldsymbol{S})$ for any $\boldsymbol{S} \in \{-1,+1\}^{m\times n}$. Actually, we need other information to judge which minimizer should be used for the above wrapped phase estimation.*

3 Branch Cut Type Sign Estimator

3.1 Transformation of Problem 1 to Another Problem

Let $J^h_{i,j}(s_{i,j},s_{i,j+1}) := \|s_{i,j+1}\boldsymbol{v}_{i,j+1} - s_{i,j}\boldsymbol{v}_{i,j}\|^2$ and $J^v_{i,j}(s_{i,j},s_{i+1,j}) := \|s_{i+1,j}\boldsymbol{v}_{i+1,j} - s_{i,j}\boldsymbol{v}_{i,j}\|^2$ in (5). Then $J^h_{i,j}$ and $J^v_{i,j}$ depend only sign changes between neighboring pairs $(s_{i,j},s_{i,j+1})$ and $(s_{i,j},s_{i+1,j})$, respectively. For a sign matrix $\boldsymbol{S} = (s_{i,j}) \in \{-1,+1\}^{m\times n}$, we define sign change matrices $\boldsymbol{C}_h = (c^h_{i,j}) \in \{0,1\}^{m\times(n-1)}$ and $\boldsymbol{C}_v = (c^v_{i,j}) \in \{0,1\}^{(m-1)\times n}$ as

$$c^h_{i,j} := \begin{cases} 0 & \text{if } s_{i,j+1} = s_{i,j}; \\ 1 & \text{if } s_{i,j+1} = -s_{i,j}, \end{cases} \tag{6}$$

and

$$c^v_{i,j} := \begin{cases} 0 & \text{if } s_{i+1,j} = s_{i,j}; \\ 1 & \text{if } s_{i+1,j} = -s_{i,j}. \end{cases} \tag{7}$$

Moreover, by defining new cost functions $\hat{J}^h_{i,j} : \{0,1\} \to \mathbb{R}_+$ and $\hat{J}^v_{i,j} : \{0,1\} \to \mathbb{R}_+$ as

$$\begin{cases} \hat{J}^h_{i,j}(0) := J^h_{i,j}(+1,+1) = J^h_{i,j}(-1,-1); \\ \hat{J}^h_{i,j}(1) := J^h_{i,j}(+1,-1) = J^h_{i,j}(-1,+1), \end{cases}$$

and

$$\begin{cases} \hat{J}^v_{i,j}(0) := J^v_{i,j}(+1,+1) = J^v_{i,j}(-1,-1); \\ \hat{J}^v_{i,j}(1) := J^v_{i,j}(+1,-1) = J^v_{i,j}(-1,+1), \end{cases}$$

Problem 1 can be replaced with Problem 2 below.

Problem 2 (Alternative expression of Problem 1) *Find* $(\boldsymbol{C}^*_h,\boldsymbol{C}^*_v) \in \{0,1\}^{m\times(n-1)} \times \{0,1\}^{(m-1)\times n}$ *minimizing*

$$\hat{J}(\boldsymbol{C}_h,\boldsymbol{C}_v) := \sum_{i=1}^{m}\sum_{j=1}^{n-1} \hat{J}^h_{i,j}(c^h_{i,j}) + \sum_{i=1}^{m-1}\sum_{j=1}^{n} \hat{J}^v_{i,j}(c^v_{i,j}) \tag{8}$$

subject to

$$c^h_{i,j} \oplus c^v_{i,j+1} \oplus c^h_{i+1,j} \oplus c^v_{i,j} = 0 \tag{9}$$

for all $i = 1,2,\ldots,m-1$ and $j = 1,2,\ldots,n-1$, where $\oplus$ denotes the exclusive disjunction, i.e., $0\oplus 0 = 1\oplus 1 = 0$ and $0\oplus 1 = 1\oplus 0 = 1$ hold.

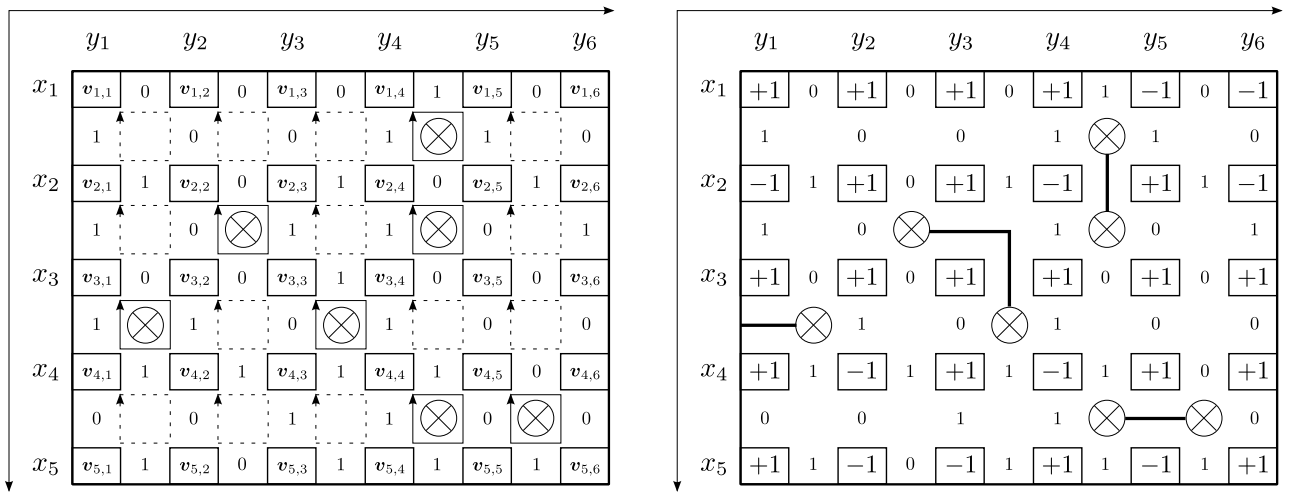

Fig. 2: Illustration of the idea of the proposed branch cut type sign estimator: (a) detection of every closed loop satisfying (10) by using the locally ideal sign changes $c^{h,\min}_{i,j}$ and $c^{h,\min}_{i,j}$ computed from $\boldsymbol{v}_{i,j}$ ($i = 1, 2, \ldots, 5$ and $j = 1, 2, \ldots, 6$) and (b) constructions of branches, sign changes $c^{h}_{i,j}$ and $c^{v}_{i,j}$, and corresponding signs $s_{i,j}$ ($i = 1, 2, \ldots, 5$ and $j = 1, 2, \ldots, 6$).

3.2 Branch Cut Type Algorithm for Solving Problem 2

To minimize (8) under condition (9), we propose the following branch cut type algorithm, which consists of steps similar to *residue detection*, *branch construction* and *path integration* steps in Goldstein's branch cut[17] for two-dimensional phase unwrapping. In what follows, assume that $\hat{J}^h_{i,j}(0) \neq \hat{J}^h_{i,j}(1)$ and $\hat{J}^v_{i,j}(0) \neq \hat{J}^v_{i,j}(1)$ for all i and j.

1. Define $c^{h,\min}_{i,j} := \mathrm{argmin}_{c\in\{0,1\}} \hat{J}^h_{i,j}(c)$ and $c^{v,\min}_{i,j} := \mathrm{argmin}_{c\in\{0,1\}} \hat{J}^v_{i,j}(c)$ as *locally ideal sign changes*. Detect every closed loop $((x_i, y_j) \to (x_i, y_{j+1}) \to (x_{i+1}, y_{j+1}) \to (x_{i+1}, y_j) \to (x_i, y_j))$ satisfying
$$c^{h,\min}_{i,j} \oplus c^{v,\min}_{i,j+1} \oplus c^{h,\min}_{i+1,j} \oplus c^{v,\min}_{i,j} = 1. \qquad (10)$$
Mark the center of such a closed loop (see Fig. 2(a)).

2. Create *branches* as shown in Fig. 2(b). Each branch is defined as a path connecting two centers marked in the first step, or a path connecting one center marked in the first step and the outside of the image. Then we can construct sign change matrices $\boldsymbol{C}_h$ and $\boldsymbol{C}_v$ satisfying condition (9) by defining
$$c^h_{i,j} := \begin{cases} c^{h,\min}_{i,j} \oplus 1 & \text{if } \begin{cases} (x_i, y_j) \text{ and } (x_i, y_{j+1}) \\ \text{lie on the left and right} \\ \text{sides of some branch;} \end{cases} \\ c^{h,\min}_{i,j} & \text{otherwise,} \end{cases}$$
and
$$c^v_{i,j} := \begin{cases} c^{v,\min}_{i,j} \oplus 1 & \text{if } \begin{cases} (x_i, y_j) \text{ and } (x_{i+1}, y_j) \\ \text{lie on the upper and lower} \\ \text{sides of some branch;} \end{cases} \\ c^{v,\min}_{i,j} & \text{otherwise.} \end{cases}$$

3. Construct a sign matrix $\boldsymbol{S}$ corresponding to the sign change matrices $\boldsymbol{C}_h$ and $\boldsymbol{C}_v$ defined in the second step, by using relations (6) and (7) (see Fig. 2(b)).

4 Numerical Experiments

We compare the effectiveness of the proposed sign estimator with that of the existing algorithm in [23] for two objects shown in Figs. 3(a) and 4(a). In both experiments, we set $\mathcal{L} := \{(x_i, y_j)\}^{i=1,2,\ldots,256}_{j=1,2,\ldots,256}$, and set $a(x, y) = 1$, $b(x, y) = 2$, and $n_1(x, y) = 0$ for all $(x, y) \in \mathcal{L}$ in (1). We generate the normalized fringe image $I(x, y)$ ($(x, y) \in \mathcal{L}$) by subtracting $\frac{1}{65536}\sum_{i=1}^{256}\sum_{j=1}^{256} I_1(x_i, y_j)$ from $I_1(x, y)$ followed by the normalization into $[-1, 1]$.

Figure 3(b) shows[1] the normalized fringe image $I(x, y)$ ($(x, y) \in \mathcal{L}$) based on the object in Fig. 3(a). Figure 3(c) shows the true sign $s(x, y) = \mathrm{sgn}(W(\phi(x, y)))$, to be estimated (see Section 2), of the noiseless wrapped phase $W(\phi(x, y))$ in Fig. 3(f). Figures 3(d) and 3(g) respectively depict the sign and the wrapped phase estimated by the algorithm in [23] using the parameters $\mu = 1$ and $\Gamma = 11$. Figures 3(e) and 3(h) respectively depict the sign and the wrapped phase estimated by the proposed method, where we construct branches by repeatedly connecting the closest pair of centers of closed loops satisfying (10). From these figures, we observe that the proposed branch cut type sign estimator achieves lower error rate ($\frac{190}{65536} \approx 0.29\%$) compared with the existing algorithm in [23] ($\frac{1053}{65536} \approx 1.61\%$) especially around the edges of the object.

Figure 4(b) shows $I(x, y)$ for the other object ("teapot" provided in MATLAB®) in Fig. 4(a). Figure 4(c) shows the sign $s(x, y)$ of $W(\phi(x, y))$ in Fig. 4(f). Figures 4(d) and 4(g) depict the sign and the wrapped phase estimated by the algorithm in [23]. Figures 4(e) and 4(h) depict the sign and the wrapped phase estimated by the proposed method. In this experiment, the proposed sign estimator achieves again lower error rate ($\frac{141}{65536} \approx 0.22\%$) compared with the existing algorithm in [23] ($\frac{1167}{65536} \approx 1.78\%$).

Acknowledgment This work was supported in part by JSPS Grants-in-Aid (26-920) and (B-15H02752).

[1] For each image in Figs. 3(b)–3(h) and 4(b)–4(h), the sample values in $[\mathrm{Min}, \mathrm{Max}]$ on $\mathcal{L}$ are rescaled into [0 (black), 255 (white)].

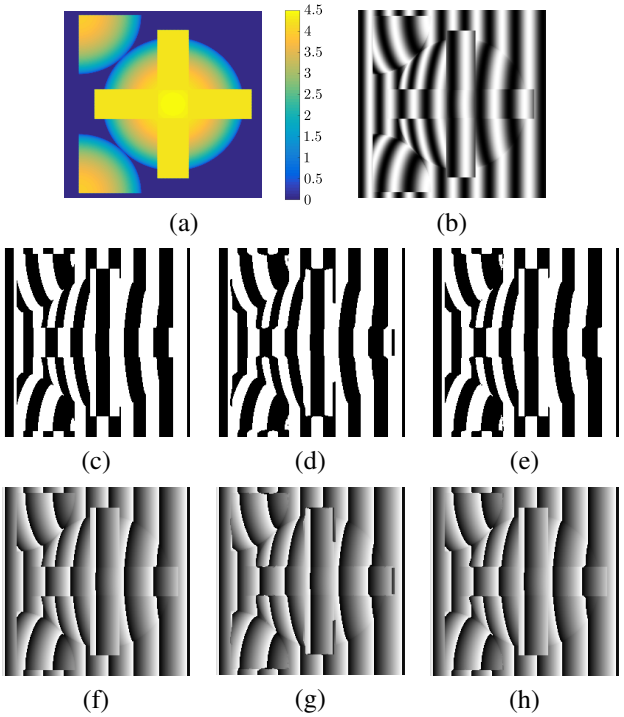

Fig. 3: Experimental results (I): (a) object, (b) $I(x, y)$, (c) $s(x, y) = \text{sgn}(W(\phi(x, y)))$ (to be estimated), (d) signs estimated by [23], (e) signs estimated by the proposed method, (f) $W(\phi(x, y))$, (g) $\phi^W(x, y)$ based on the signs in (d), and (h) $\phi^W(x, y)$ based on the signs in (e).

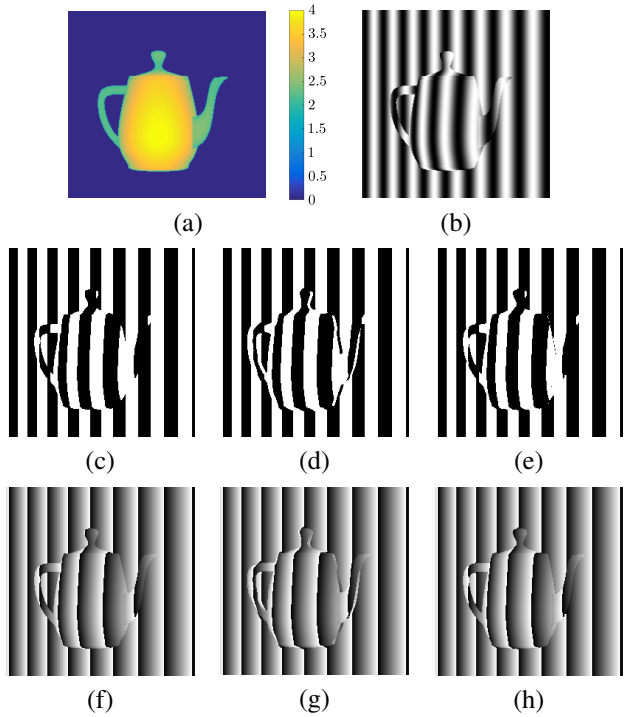

Fig. 4: Experimental results (II): (a) object, (b) $I(x, y)$, (c) $s(x, y) = \text{sgn}(W(\phi(x, y)))$ (to be estimated), (d) signs estimated by [23], (e) signs estimated by the proposed method, (f) $W(\phi(x, y))$, (g) $\phi^W(x, y)$ based on the signs in (d), and (h) $\phi^W(x, y)$ based on the signs in (e).

References

1) D. Malacara: *Optical Shop Testing*, 3rd ed, Wiley (2007)
2) S. S. Gorthi and P. Rastogi: Fringe projection techniques: Whither we are?, *Opt. Lasers Eng.*, **48**-2, 133/140 (2010)
3) S. Zhang: Recent progresses on real-time 3D shape measurement using digital fringe projection techniques, *Opt. Lasers Eng.*, **48**-2, 149/158 (2010)
4) F. Lilley, M. J. Lalor, and D. R. Burton: Robust fringe analysis system for human body shape measurement, *Opt. Eng.*, **39**-1, 187/195 (2000)
5) L. C. Chen and C. C. Huang: Miniaturized 3D surface profilometer using digital fringe projection, *Meas. Sci. Technol.*, **16**-5, 1061/1068 (2005)
6) K. Genovese and C. Pappalettere: Whole 3D shape reconstruction of vascular segments under pressure via fringe projection techniques, *Opt. Lasers Eng.*, **44**-12, 1311/1323 (2006)
7) M. de Angelis, D. de Nicola, P. Ferraro, A. Finizio, and G. Pierattini: Liquid refractometer based on interferometric fringe projection, *Opt. Commun.*, **175**-4–6, 315/321 (2000)
8) C. Quan, C. J.Tay, X. Y. He, X. Kang, and H. M. Shang: Microscopic surface contouring by fringe projection method, *Opt. Lasers Eng.*, **34**-7, 547/552 (2002)
9) J. Burke, T. Bothe, W. Osten, and C. F. Hess: Reverse engineering by fringe projection, *Proc. SPIE*, **4778**, 312/324 (2002)
10) S. Tan, D. Song, and L. Zeng: A tracking fringe method for measuring the shape and position of a swimming fish, *Opt. Commun.*, **173**-1–6, 123/128 (2000)
11) F. Yuan, D. Song, L. Zeng: Measuring 3D profile and position of a moving object in large measurement range by using tracking fringe pattern, *Opt. Commun.*, **196**-1–6, 85/91 (2001)
12) J. Yagnik, G. S. Siva, K. R. Ramakrishnan, and L. K. Rao: 3D shape extraction of human face in presence of facial hair: A profilometric approach, *Proc. IEEE TENCON*, 1/5 (2005)
13) S. Huang, Z. Zhang, Y. Zhao, J. Dai, C. Chen, Y. Xu, E. Zhang, L. Xie: 3D fingerprint imaging system based on full-field fringe projection profilometry, *Opt. Lasers Eng.*, **52**, 123/130 (2014)
14) K. Creath: Phase-measurement interferometry techniques, *Prog. Opt.*, **26**, 349/393 (1988)
15) D. C. Ghiglia and M. D. Pritt: *Two-Dimensional Phase Unwrapping: Theory, Algorithms, and Software*, Wiley (1998)
16) L. Ying: Phase unwrapping, *Wiley Encyclopedia of Biomedical Engineering, 6-Volume Set*, Wiley (2006)
17) R. M. Goldstein, H. A. Zebker, and C. L. Werner: Satellite radar interferometry: Two-dimensional phase unwrapping, *Radio Sci.*, **23**-4, 713/720 (1988)
18) D. Kitahara and I. Yamada: Algebraic phase unwrapping based on two-dimensional spline smoothing over triangles, *IEEE Trans. Signal Process.*, **64**-8, 2103/2118 (2016)
19) D. Wu and K. L. Boyer: Sign ambiguity resolution for phase demodulation in interferometry with application to prelens tear film analysis, *Proc. IEEE CVPR*, 2807/2814 (2010)
20) M. Servin, J. L. Marroquin, and F. J. Cuevas: Demodulation of a single interferogram by use of a two-dimensional regularized phase-tracking technique, *Appl. Opt.*, **36**-19, 4540/4548 (1997)
21) J. A. Quiroga, M. Servin, and F. J. Cuevas: Modulo 2π fringe orientation angle estimation by phase unwrapping with a regularized phase tracking algorithm, *J. Opt. Soc. Am. A*, **19**-8, 1524/1531 (2002)
22) C. J. Tay, C. Quan, F. J. Yang, and X. Y. He: A new method for phase extraction from a single fringe pattern, *Opt. Commun.*, **239**-4–6, 251/258 (2004)
23) J. Villa, I. De la Rosa, G. Miramontes, and J. A. Quiroga: Phase recovery from a single fringe pattern using an orientational vector-field-regularized estimator, *J. Opt. Soc. Am. A*, **22**-12, 2766/2773 (2005)
24) H. Wang and Q. Kemao: Frequency guided methods for demodulation of a single fringe pattern, *Opt. Express*, **17**-17, 15118/15127 (2009)
25) C. Tian, Y. Yang, D. Liu, Y. Luo, and Y. Zhuo: Demodulation of a single complex fringe interferogram with a path-independent regularized phase-tracking technique, *Appl. Opt.*, **49**-2, 170/179 (2010)
26) J. A. Quiroga, J. A. Gómez-Pedrero, and Á. García-Botella: Algorithm for fringe pattern normalization, *Opt. Commun.*, **197**-1–3, 43/51 (2001)
27) J. O. Ramsay and B. W. Silverman: *Functional Data Analysis*, Springer (2005)